

09,08

Peculiarities of changes in the intensities of the main photoluminescence bands of Tb³⁺ ions and their satellites in polycrystalline Gd₂O₃:Tb(3 mol%)

© V.V. Bakovets, P.E. Plyusnin, I.V. Jushina, M.I. Rakhmanova, A.V. Sotnikov,
I.P. Dolgovesova, T.D. Pivovarova

Nikolaev Institute of Inorganic Chemistry, Siberian Branch, Russian Academy of Sciences,
Novosibirsk, Russia

E-mail: becambe@niic.nsc.ru

Received March 17, 2023

Revised March 17, 2023

Accepted March 28, 2023

Samples of Gd₂O₃:Tb(3 mol%) phosphor were obtained by sol-gel method followed by annealing at 800°C and 1200°C in air. At high annealing temperature, the intensities of the main emission bands 484 and 541 nm increase, but the ratio of the intensities of these emission bands to their satellites 493 and 549 nm respectively decreases. Based on the analysis of X-ray diffractometry, emission spectra, far-infrared and Raman spectroscopy, as well as diffuse reflectance spectroscopy, we established: the increase in the crystallinity of the samples with a significant reduction of the lattice strain stress at elevated annealing temperatures, changes in the structure of the bandgap with degenerated acceptor and donor zones of impurities Tb⁴⁺ and Tb³⁺ respectively. The diffuse reflection spectra of the sample after annealing at 800°C under optical excitation showed a direct charge transition through the bandgap with $E_g = 2.56$ eV. After elevated annealing temperature the concentration of Tb⁴⁺ ions decreases due to reduction to Tb³⁺. As a result, at low excitation energies the degeneracy of the acceptor zone is still preserved and there is a direct transition of charges through the bandgap with $E_g = 2.55$ eV. At high excitation energies the degeneracy of the acceptor zone is removed and there is a direct transition through the bandgap with $E_g = 3.39$ eV. These effects are accompanied by a relatively large increase in the emission intensity of the satellites, especially at the 549 nm.

Keywords: Gd oxide, Tb³⁺ photoluminescence spectra, far infrared and Raman spectroscopy spectra, structure of the bandgap, distribution of Tb³⁺ and Tb⁴⁺ in cation sublattice.

DOI: 10.21883/PSS.2023.05.56053.37

1. Introduction

Lanthanide and yttrium oxides are traditional matrices for luminescent materials with intracenter emission [1]. These materials are characterized by chemical and thermal stability in air and maintain their photoluminescent (FL) properties under intense solar radiation. Such FL are used for illuminated panels and indicators, color cathodoluminescent tubes and screens. FL X-ray excitation enables these materials to be used in medical X-ray equipment, in particular matrixes doped with terbium activator due to their pleasant green and high-intensity luminescence. A widely used FL activator — Tb³⁺, during material synthesis in air, which is technologically acceptable in mass production, is partially represented by Tb⁴⁺ ionic form [2] that has no FL. This reduces the optical efficiency of such material. In addition, ~ 490 and ~ 550 nm main emission bands in the FL spectra of materials are represented by doublets whose nature has no rigorous proof. However, when selecting a pure green or blue standard, i.e. a color with a narrow emission band, any main band satellites induce high uncertainties, particularly as the intensity ratio of the doublet bands varies with material and even within a single material, which prepared in a different synthesis conditions [1–6],

and with different FL excitation wavelenths [7]. This is associated, among other things, with the sensitivity of Tb³⁺ to the immediate environment [8], especially to the excess oxygen content in TbO_{1.5+x} [2] and with FL excitation transmission efficiency from the environment to the ion activator. Interestingly, doublets are observed in inorganic products, but they are absent in organic acid salts (e.g. terbium oleate) [9]. In this case, occurrence of doublets is attributed to the influence of surface states, in particular formation of 548 nm satellite. Presence of Tb⁴⁺ has not been studied. Correlation of doublet occurrence with an increase in crystallite sizes with an annealing temperature rise was observed in [2]. In this case, reduced Tb⁴⁺ content was recorded. In addition, it should be noted that a cubic modification with a bixbyite type lattice generated at low synthesis and annealing temperatures is more acceptable in terms of process. This modification is characterized by three Ln³⁺ positions, including Tb³⁺ activator, in centrosymmetric C_{3i} and noncentrosymmetric C_2 positions, and in surface states of C_S at the crystallite boundaries in a polycrystalline material. Since all emission bands, including satellite bands, are relative narrow, then the resulting color shades are often not reproduced on some screens and color standardization with respect to day light is ultimately

degraded. Thus, color of a screen may be perceived in a way not often favorable to eye, e.g. the warm — cold light effect.

Therefore, the purpose of this study is to address spectral features of $\text{Gd}_2\text{O}_3:\text{Tb}(3\text{ mol}\%)$ FL phosphor associated with the nature of distribution of Tb^{3+} FL activator and accompanying non-luminescent Tb^{4+} among three positions in the cation sublattice with a change in the annealing temperature conditions according to FL spectra analysis, far infrared (FIR) and Raman-scattering spectroscopies (RSS) as well as diffuse reflectance spectroscopy.

2. Experimental

$\text{Gd}_2\text{O}_3:\text{Tb}^{3+,4+}(3\text{ mol}\%)$ samples were prepared using a sol-gel method [10]. For the purpose of the study, $\text{Gd}(\text{NO}_3)_3 \cdot 6\text{H}_2\text{O}$ and $\text{Tb}(\text{NO}_3)_3 \cdot 5\text{H}_2\text{O}$ obtained from the corresponding oxides and containing at least 99.9% of the main component were used as reagents. Two-fold excess of „extra pure“ grade NaOH solution in double-distilled water was used as a precipitator. The synthesis was performed using a setup with initial reagents sprayed in order to achieve high sol dispersion and homogeneity of components in the stock solution. The obtained $(\text{Gd}_{0.97}\text{Tb}_{0.03})_x(\text{OH})_y(\text{CO}_3)_z \cdot n(\text{H}_2\text{O})$ residue was washed out to neutral pH of the washing water and air dried at 50°C . Then the samples were annealed at 800 and 1200°C during 1 h until $\text{Gd}_2\text{O}_3:\text{Tb}^{3+,4+}(3\text{ mol}\%)$ end products were formed with a total absence of water in accordance with IR spectroscopy. Content of Na impurity in the end oxide according to chemical analysis is $< 5 \cdot 10^{-2}\text{ wt}\%$, content of rare earths is $< 1 \cdot 10^{-2}\text{ wt}\%$, balance is $10^{-3}\text{--}10^{-4}\text{ wt}\%$. Tb 3 mol% was selected because at 1–1.5 mol% Tb concentration quenching of FL [8,11] starts due to exchange interactions of these ions. This met the purpose of the study, i.e. investigation of the influence of FL activator ion exchange interactions on the formation of main FL band doublets.

Weight loss and differential scanning calorimetry (DSC) of samples with temperature increase up to 1200°C were studied using NETZSCH STA 449F instrument. Heating rate was $10\text{ K} \cdot \text{min}^{-1}$ in $\text{Ar}/\text{O}_2(20\text{ vol}\%)$ atmosphere.

X-ray diffraction analysis of samples was carried out using Shimadzu XRD-7000 (CuK_α -emission, Ni-filter diffractometer, range $5\text{--}70^\circ 2\Theta$, interval 0.03° , uptake 2 s). For details of synthesis procedure and X-ray diffraction analysis and FL spectroscopy, see [10].

Luminescence spectra were studied using VARIAN Cary Eclipse fluorescent spectrophotometer. Excitation wavelength was selected according to diffuse reflectance spectra (DRS) and luminescence excitation spectra (SVL) of the main bands of Tb^{3+} emission doublet 542 nm. According to the DRS experiments, all polycrystalline samples have high ultraviolet optical absorption about 70–80%. The excitation wavelength of $\lambda_{\text{ex}} = 265\text{ nm}$ was selected according to the excitation energy transfer via the known channels:

charge transfer $\text{Gd}^{3+} \rightarrow \text{Tb}^{3+}$ charges and electron transfer $4f \rightarrow 5d \text{ Tb}^{3+}$ [5,12].

FIR spectra were recorded using VERTEX 80v spectrometer with spectral resolution of 0.2 cm^{-1} . Powder samples were ground with PE-spectral polyethylene and pressed in the form of tablets. FIR spectra were recorded in pure dry nitrogen atmosphere. RSS spectra were recorded using Spex Triplemate spectrometer at Ar laser excitation wavelength 488 nm.

Diffuse reflectance spectra (DR) $R_d = F(\lambda)$ of powders were recorded by a standard method using Shimadzu UV-3101PC spectrophotometer in the wavelength range λ from 240 to 800 nm. UV and visible range wavelength axis calibration accuracy was $\pm 0.3\text{ nm}$, wavelength reproducibility was $\pm 0.1\text{ nm}$. Measurement errors caused by light scattering were 0.01%. BaSO_4 was used as a reference standard.

3. Experimental results

3.1. Structural analysis

X-ray diffraction patterns of the samples are shown in Figure 1 and correspond to the standard structure of cubic $\text{C-Gd}_2\text{O}_3$ ICSD-183130 (ICSD-96207).

Reflections of $\text{C-Gd}_2\text{O}_3:\text{Tb}(3\text{ mol}\%)$ — 800°C sample feature large width at half maximum and high baseline excitation. high content of amorphous phase represented at small angles 2θ is observed. The table shows crystallographic parameters of the obtained samples.

Lattice constant decreases with higher sample annealing temperature. This should have been expected, because stoichiometric coefficient x for oxygen in TbO_x decreases with $x = 1.71$ (Tb_7O_{12}) [2] or $x = 1.75$ (Tb_4O_7) [13] with annealing in air up to 800°C and achieves $x = 1.5$ with annealing in air at 1200°C with increased annealing time due to Tb^{4+} reduction to Tb^{3+} [2,13,14]. In addition, at

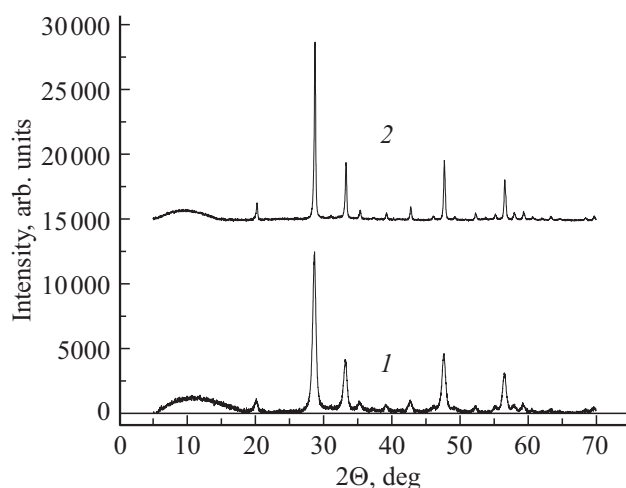


Figure 1. X-ray diffraction patterns of $\text{Gd}_2\text{O}_3:\text{Tb}(3\text{ mol.}\%)$ samples. Annealing at 800°C (1) and 1200°C (2).

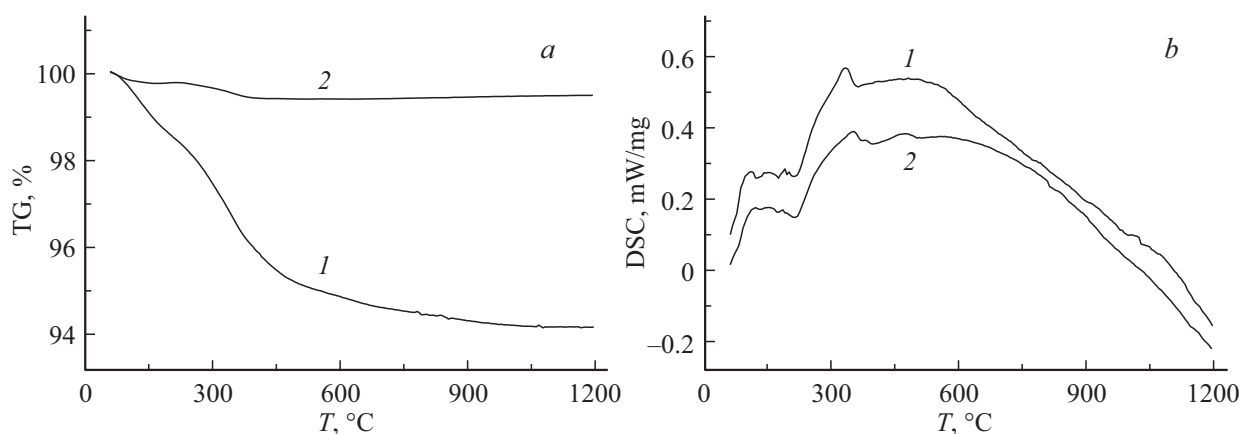


Figure 2. Thermal analysis curves for Gd₂O₃:Tb³⁺ (3 mol%) samples annealed at 800 (1) and 1200°C (2). Weight loss (a), DSC results (b).

Crystallographic parameters: phase composition, lattice constants a , coherent scattering region CSR_{H-W} and strain ϵ

Sample	Phase composition	a , Å	CSR _{H-W} = d_{cr} , nm	ϵ
Gd ₂ O ₃ :Tb(3%) 800°C	Cubic C-Gd ₂ O ₃	10.815(2)	20 ± 3	0.1635 ± 0.0081
Gd ₂ O ₃ :Tb(3%) 1200°C	Cubic C-Gd ₂ O ₃	10.787(2)	75 ± 8	0.0535 ± 0.0026

Note. Reference cell parameter: C-Gd₂O₃ a = 10.81 Å ICSD-96207.

high temperature, Tamman's lattice atom mobility increase effect is initiated when metastable cubic lattice begins to transform into a monoclinic lattice [10]. Actually, the lattice cell volumes and ratio $V_M/V_C = 436/1263$ (ICSD 184528 and ICSD 96207) are such that 72.666 Å³ and 78.995 Å³ fall within one formula unit, respectively. Moreover, the amount of deformations on the crystallite boundaries with annealing at 1200°C is reduced by a factor of ~ 3 (Table) due to the increased crystallite sizes and reduced specific area of crystallites [15].

3.2. Thermal analysis

Figure 2 shows the change in weight and thermal effects during thermogravimetric analysis of both samples after long-term storage.

The sample prepared at a lower temperature apparently has a higher weight loss and exhibits more intense thermal effects at the initial heating stage. These changes meet the previously presented findings for TbO_x [2]. At the first stage, weight loss is observed due to evaporation of absorbed water, removal of absorbed carbonate ions and dehydroxylation to 300°C followed by overlapping between the process of hydroxycarbonate structure transformation into C-Gd₂O₃:Tb oxide form and exo-effect. Low weight loss indicates impurity content of these components. At the second heating stage, when only endo-effect is clearly

exhibited, Tb⁴⁺ are reduced to Tb³⁺ in accordance with the known effects of terbium oxide annealing in air [2,13,14].

3.3. Photoluminescence

Figure 3 shows VL excitation spectra at $\lambda_{em} = 543$ nm and FL spectra at excitation $\lambda_{ex} = 265$ nm of samples annealed at 800 and 1200°C.

The spectra are normalized by FL intensity of Gd₂O₃:Eu(3.5 mol%) standard. Emission intensity of all peaks is higher after annealing at 1200°C. The main emission peaks of ⁵D₄ → ⁷F₆ and ⁵D₄ → ⁷F₅ transitions of Tb³⁺ are represented by doublets in ranges 482–491 and 541–549 nm, respectively. The presence of doublets is allegedly associated with splitting of the main emission levels into sublevels [5] or with the involvement of phonons [3]. The intensity ratio of the main emission changes from $I_{543}/I_{548} = 2.1$ at 800°C to $I_{541}/I_{550} = 1.22$ at 1200°C; from $I_{543}/I_{489} = 3.5$, $I_{548}/I_{493} = 2.3$ at 800°C to $I_{541}/I_{484} = 2.7$, $I_{550}/I_{492} = 2.4$ at 1200°C. After annealing at 1200°C, the excitation energy transfer is apparently increased from transition ⁵D₄ → ⁷F₆ to ⁵D₄ → ⁷F₅ from 489 nm band to 541 nm band. Band doublets are typically observed in the blue and green bands. And the ratios of the doublet components decrease with an increase in annealing temperature. Doublet intensity sums $I_{543} + I_{548} = 541$ and $I_{489} + I_{493} = 181$ and ratio 541/181 = 3.0 at 800°C, $I_{541} + I_{550} = 15222$ and $I_{484} + I_{492} = 5958$ and ration 2.6

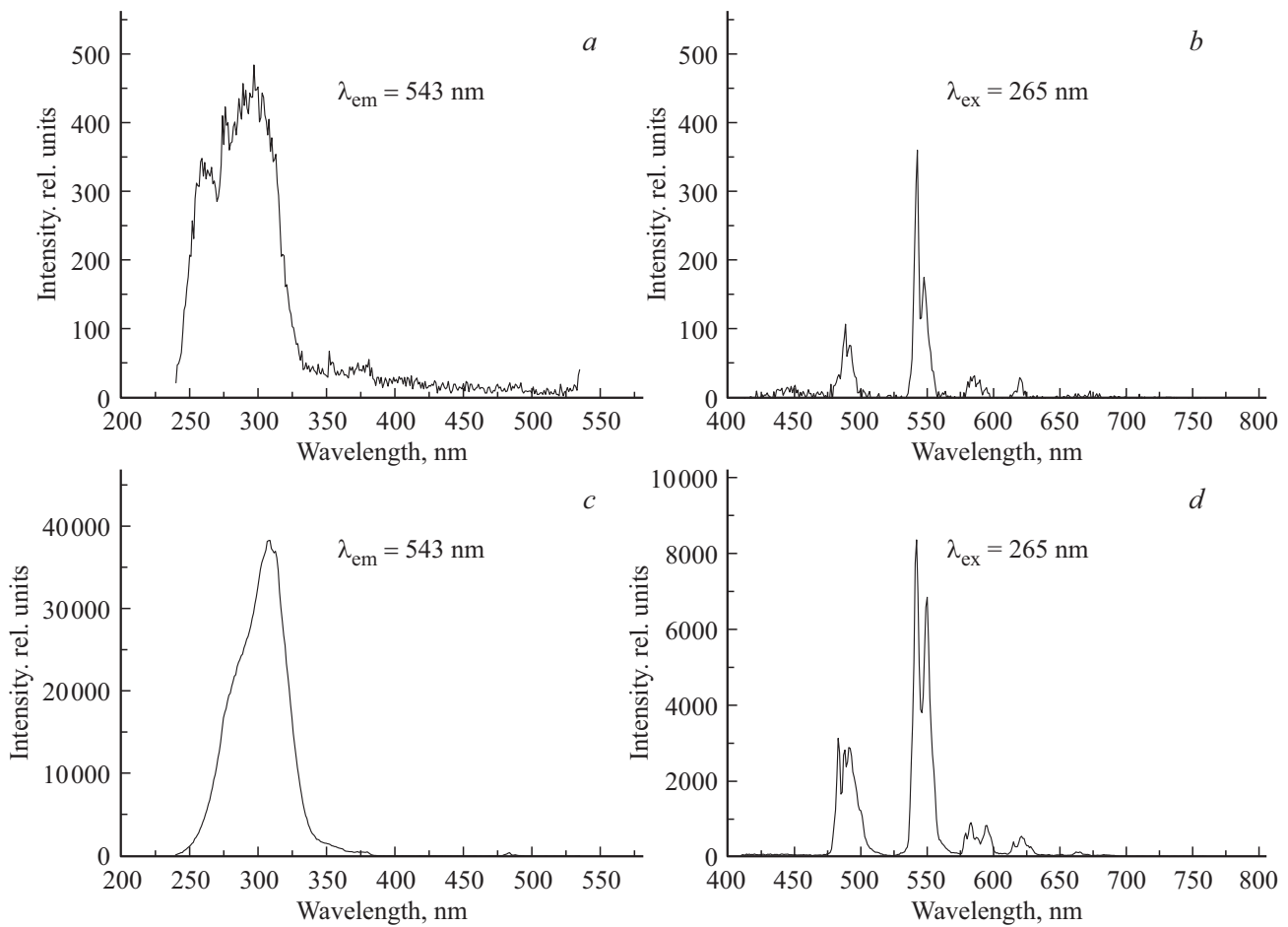


Figure 3. VL (*a, c*) and FL (*b, d*) spectra of $C\text{-Gd}_2\text{O}_3:\text{Tb}^{3+}$ (3 mol%) samples annealed at 800 (*a, b*) and 1200°C (*c, d*).

at 1200°C. Total emission transition energy ratio (by the sum of doublet intensities)

$$\frac{[E(^5D_4 \rightarrow ^7F_6)[I_{484} + I_{492}] + E(^5D_4 \rightarrow ^7F_5)[I_{541} + I_{550}]]_{1200^\circ\text{C}}}{[E(^5D_4 \rightarrow ^7F_6)[I_{489} + I_{493}] + E(^5D_4 \rightarrow ^7F_5)[I_{543} + I_{548}]]_{800^\circ\text{C}}} = 0.87.$$

Ratio of total doublet energies of the similar emission transitions at different annealing temperatures

$$\sum_{\sim 550}^{1200^\circ\text{C}} / \sum_{\sim 550}^{800^\circ\text{C}} = 28 \quad \text{and} \quad \sum_{\sim 490}^{1200^\circ\text{C}} / \sum_{\sim 490}^{800^\circ\text{C}} = 33.$$

Thus, if with annealing at 1200°C, the total intensity of [484 + 492] nm bands increases substantially with respect to annealing at 800°C, then relatively lower energy is transferred to emission transition $^5D_4 \rightarrow ^7F_5$. In addition, energy transfer to transition $^5D_4 \rightarrow ^7F_5$ (550 nm) prevails over the transfer to transition 7F_5 (541 nm) at 1200°C. Change in energy ratio of FL band doublets may be associated with a short-range order change which takes place with defectness variation of the crystallite (Table), and with redistribution of Tb^{3+} FL activator over cation sublattices with symmetry C_{3i} , C_2 and surface states C_5

and, in addition, due to the change in reduction of some Tb^{4+} to Tb^{3+} with sample annealing in air at different temperatures. It seems that short-range order changes of crystal lattice shall exhibit in far IR spectroscopy (FIR) and Raman scattering spectroscopy (RSS).

3.4. Far IR spectroscopy

Figure 4 shows FIR spectra of $\text{Gd}_2\text{O}_3:\text{Tb}$ (3 mol%) test samples and for comparison spectra $\text{Gd}_2\text{O}_3:\text{Tb, Eu}$ (2.5 mol%) studied before [16] after annealing in air and in H_2 .

The shown spectra are almost similar by absorption band layout, but their intensity ratio is changed (Figure 4, *a, b*). It can be seen that 498 nm peak (Figure 4, *b*) detected for $\text{Gd}_2\text{O}_3:\text{Tb, Eu}$ (2.5 mol%) with annealing at 1200°C in air has disappeared and intensity of annealing in H_2 is a little lower. The spectra feature lower intensity of A region bands 100–250 cm^{-1} reflecting translatory motions of cations in C_{3i} position (100–140 cm^{-1}) and C_2 position (150–250 cm^{-1}) [17–19], high intensity of B region bands of torsion and deformation vibrations 250–400 cm^{-1} ((Ln-O₆ octahedron internal vibration region), primarily vi-

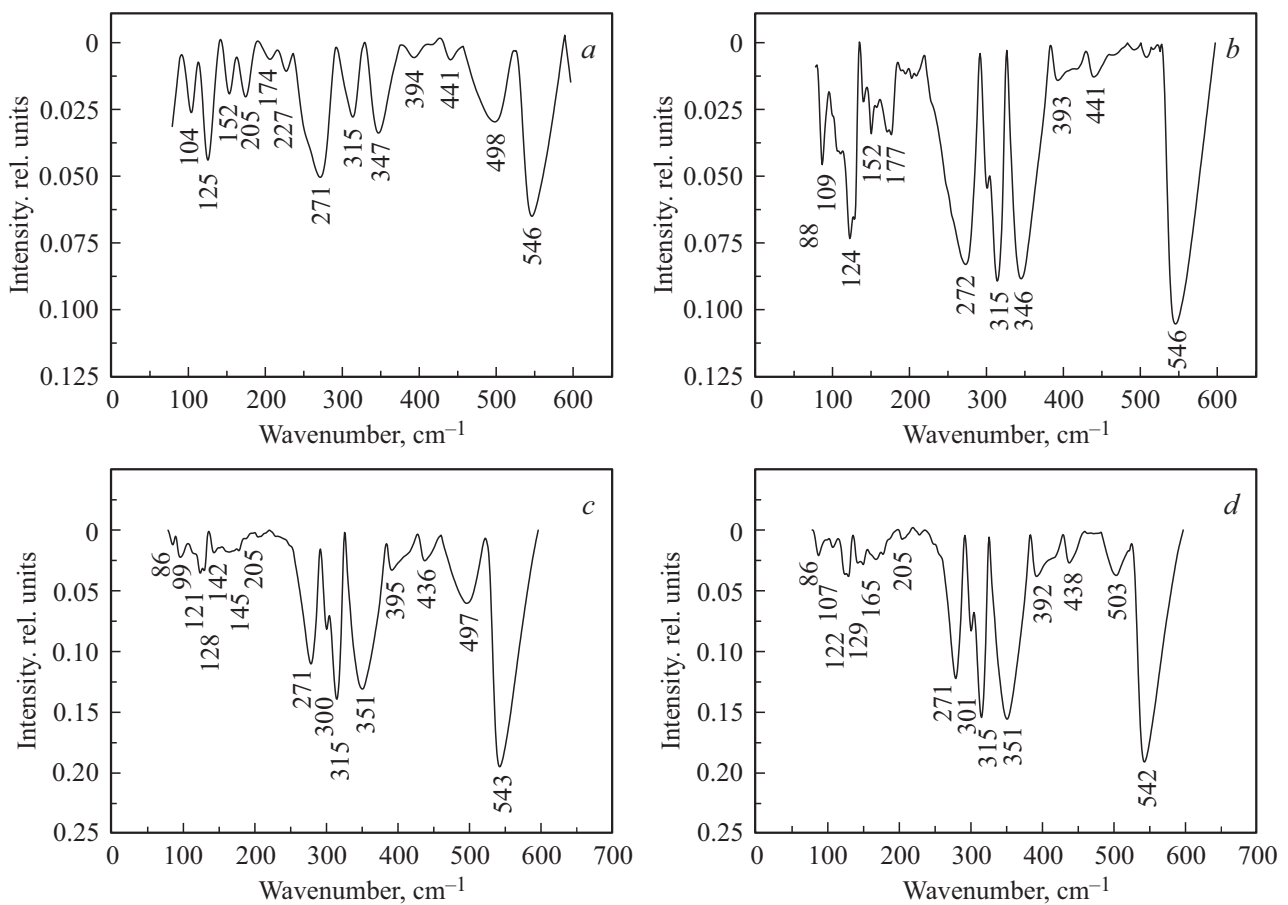


Figure 4. FIR spectra of Gd₂O₃:Tb(3 mol%) samples after annealing in air at 800°C (a) and 1200°C (b); of Gd₂O₃:Tb,Eu(2.5 mol%) samples after annealing at 1200°C in air (c) and in H₂ atmosphere (d).

brations of O²⁻ [14,17,20] (Figure 4, a, b) and high intensity of C region bands 450–600 cm⁻¹ (intraoctahedron Ln-O stretching region [18,21]. Band intensity slightly increases with annealing at high temperature of 1200°C. However, 315 and 347 cm⁻¹ bands are 3 times larger and 498 cm⁻¹ band has almost disappeared. It should be noted that the appearance of 142 cm⁻¹ band may be attributed to the motion of Tb³⁺ in the centrosymmetric position. This band was assigned to C_{3i} position [19] for the related Gd₂O₃:Tb,Eu(2.5 mol%) compound.

3.5. Raman spectroscopy

Figure 5 shows the Raman spectra of Gd₂O₃:Tb(3 mol%) samples annealed at 800 and 1200°C and, for comparison, of Gd₂O₃:Tb,Eu(2.5 mol%) sample.

Like for FIR spectra, three regions with typical change in band intensity and, to a lesser extent, with position of their wave number maxima are observed for RSS spectra. These regions cover the following wave number ranges: region A — 100–250, B — 300–440 and C — 450–600 cm⁻¹. When the spectra are represented in a normalized form by the most intense RSS band ~ 360 cm⁻¹ for individual cubic Gd and Tb oxides[22] (in this case,

it is 363 cm⁻¹ band for the major cations of Gd matrix), then region A and C bands after sample annealing at 1200°C are apparently much more intense than the bands of the sample annealed at 800°C. Therefore, the Raman shift bands reflecting the cation motion (region A) and stretching vibrations (region C) are much more intense after high-temperature annealing. These effects seem to be associated with considerable increase of crystallinity of the sample annealed at 1200°C (Table). This is probably accompanied with a higher polarization of atomic bonds in regions A and C when the degree of short-range ordering increases by the excitation with 488 nm argon laser.

3.6. Diffuse reflection

Figure 6 shows diffuse reflection spectra of the samples.

As can be seen the spectra of the samples annealed at different temperatures differ considerably. With annealing at 800°C, the absorption coefficient is higher throughout the UV and visible ranges reflected light flux. Reflection dependence profile $R_d = f(W.n)$ is shown by a smooth S-shape curve which is linearized near the absorption edge in Tauc coordinates $(F(R_d)h\nu)^2 - h\nu$ with high regression coefficient $R^2 = 0.9954$, which corresponds to a direct

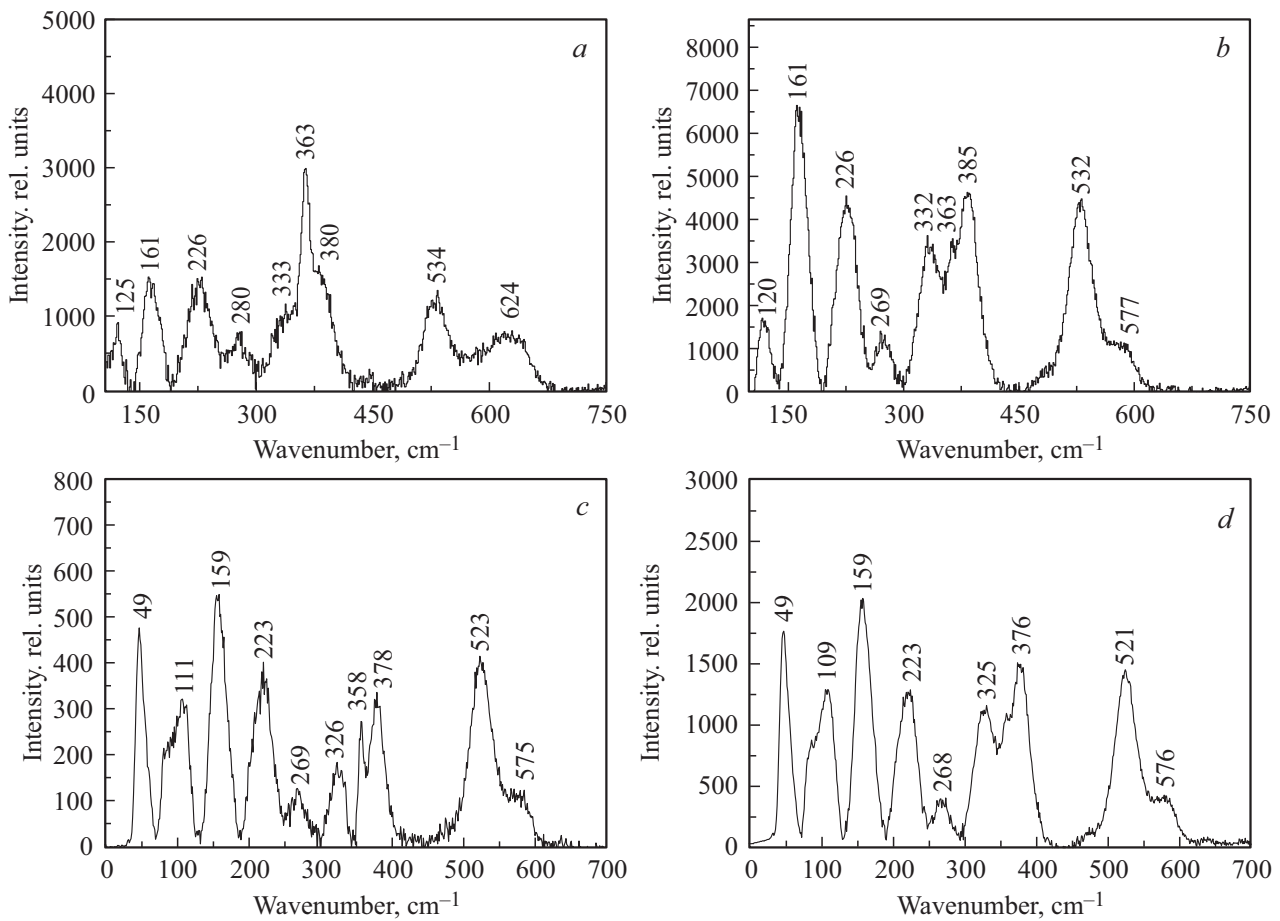


Figure 5. RSS spectra of $\text{Gd}_2\text{O}_3:\text{Tb}(3 \text{ mol}\%)$ samples annealed at 800°C (a) and 1200°C (b), and of $\text{Gd}_2\text{O}_3:\text{Tb},\text{Eu}(2.5 \text{ mol}\%)$ samples annealed at 1200°C in air (c) and in H_2 atmosphere (d).

charge transition via the band gap (BG) [24]. $F(R_d)$ is the optical absorption parameter in Kubelka–Munk model [25]. The corresponding BG width E_g is equal to 2.56 eV. A close value was recorded for $\text{C-Tb}_2\text{O}_3$ films with $E_g = 2.7 \text{ eV}$ [26].

For the sample annealed at 1200°C , it is apparent that BG structure is more sophisticated and is divided into two zones which are linearized in coordinates $(F(R_d)h\nu)^2 - h\nu$ with $E_g = 2.55 \text{ eV}$, $R^2 = 0.9946$ for a long-wavelength zone and $E_g = 3.39 \text{ eV}$, $R^2 = 0.9902$ for a short-wavelength zone. Existence of two zone of this kind $R_d = f(h\nu)$ for TbO_x samples has been also detected before [13,27]. Function $R_d = f(h\nu)$ for Gd_2O_3 samples is represented in the addressed energy region $4.96 > h\nu > 1.77 \text{ eV}$ by a straight line [27] falling into the highest energy region. Thus, a two-zone form of $R_d = f(h\nu)$ for the studied $\text{Gd}_2\text{O}_3:\text{Tb}(3 \text{ mol}\%)$ samples is defined by Tb^{3+} and Tb^{4+} impurities rather than by the matrix.

4. Discussion of findings

The BG structure behavior taking into account the actual crystal lattice structure and concentration of Tb^{3+} and Tb^{4+}

dopants make it possible to describe the following charge transfer mechanism at the UV absorption band edge. When $\text{Gd}_2\text{O}_3:(\text{Tb}^{3+} + \text{Tb}^{4+}) 3 \text{ mol}\% \equiv \text{Gd}_2\text{O}_3:\text{Tb}^{3.5+}$ sample is annealed at 800°C in air [2], high concentration of Tb^{4+} and Tb^{3+} ($C_{\text{Tb}^{4+}} < C_{\text{Tb}^{3+}} \sim 10^{20} \text{ cm}^{-3}$) is maintained. However, the terbium oxide composition meets the proportion $\text{TbO}_{1.71}$. Tb^{4+} impurity ions are p -type dopants in $\text{C-Gd}_2\text{O}_3$ matrix and form a degenerate zone at the valence band top. Tb^{3+} are n -type dopants and form a degenerate zone at the conduction band bottom. With high concentrations ($> 1.5 \text{ mol}\%$), the adjacent ions exhibit exchange interactions [2,11]. According to Kubelka–Munk-Tauc model processing (Figure 6, b), charge transitions between the p -type and n -type degenerate zones are straight. Optical band gap E_g is 2.56 eV.

When the sample is annealed at 1200°C , concentration of Tb^{4+} decreases dramatically to [2] $\text{TbO}_{1.53}$. And the BG structure is changed with an increase in the exciting light flux quantum energy and forms two BG overcome energy regions. Both segments of the corresponding functional dependences are linearized in coordinates $(F(R_d)h\nu)^2 - h\nu$, which corresponds to direct charge transitions via BG. Low-energy region is characterized by $E_g = 2.55 \text{ eV}$, which

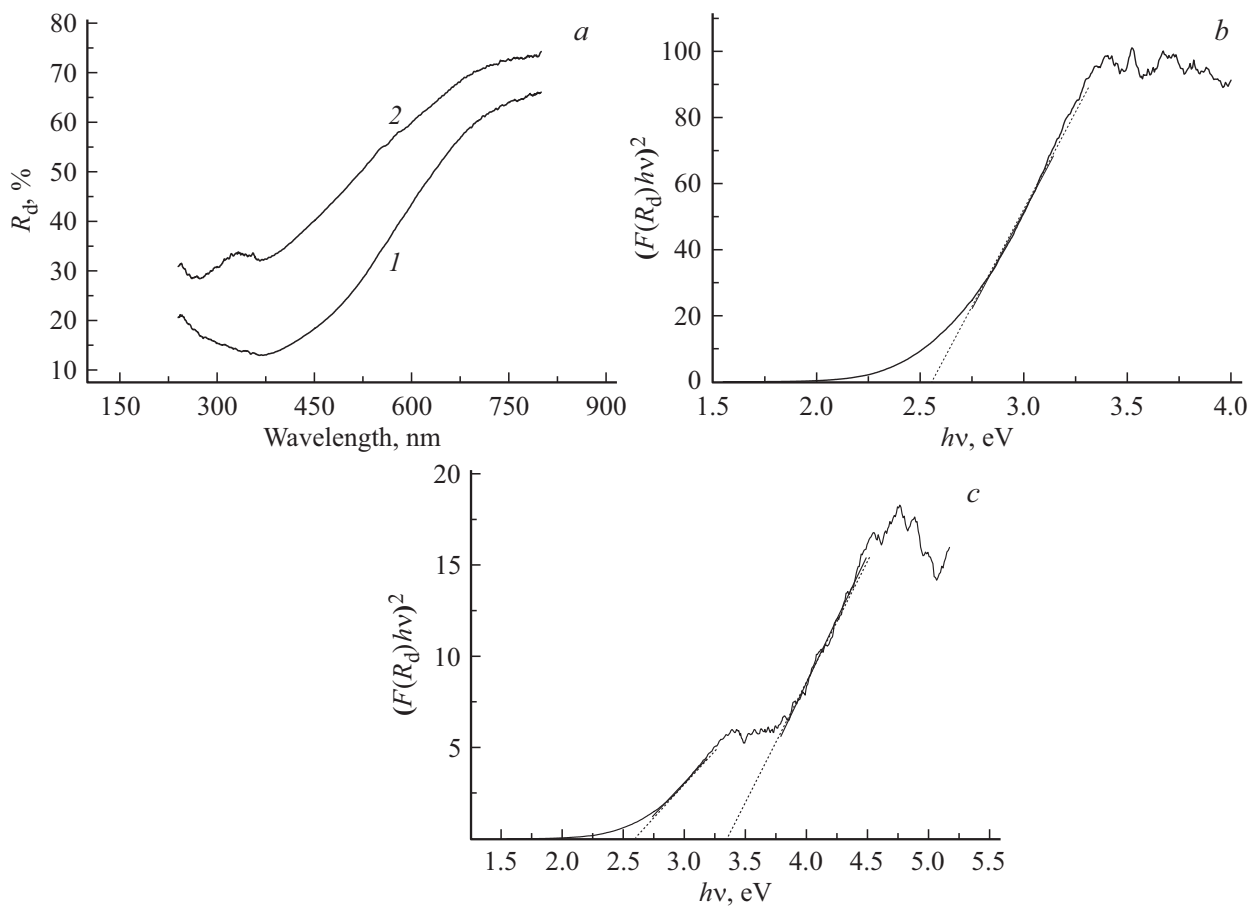


Figure 6. Diffuse reflectance spectra of the samples (a) annealed at 800 — 1 and 1200°C — 2, absorption spectra in Tauc coordinates [23] annealed at 800 (b) and 1200°C (c).

corresponds with that for the sample annealed at 800°C. This indicates that the degeneration of Tb^{4+} p -type dopant zone is maintained. With transition to high-energy optical excitation region, the degeneration of this zone is removed by means of charge re-compensation between the p -type and n -type zones, but the degeneration of Tb^{3+} n -type dopant subzone is maintained due to high ion concentration. The corresponding E_g increases up to 3.4 eV. The n -type zone degeneration is not removed, because E_g does not achieve the value typical for the intrinsic absorption of $C-Gd_2O_3$ matrix $E_g = 5.45$ eV [28,29]. It is known that for TbO_x : from $x = 1.5$ to $x = 1.53$ $E_g = 3.88$ eV and with further increase, E_g gradually decreases [13]. It is not unlikely that BG contains a Tb^{3+} surface state zone that is formed with Tb^{4+} transition into C_{3i} position, which is a little deformed by the crystallite boundary proximity, followed by reduction to Tb^{3+} during annealing at 1200°C. However, this zone may overlap the main n -type zone. For systems with n -type and p -type dopants, two Fermi levels often occur. For the system of interest, two Fermi levels may not occur, because concentrations of Tb^{3+} and Tb^{4+} are bound by the chemical equilibrium constant for annealing in air at the specified temperature and by charge re-

compensation for optical excitation when diffusion reflection spectrum R_d is recorded.

With transition from 800 to 1200°C, intensity ratio of doublet FL-bands for $^5D_4 \rightarrow ^7F_5$ changes from $I_{543}/I_{547} = 2.1$ to $I_{543}/I_{547} = 1.22$ and for $^5D_4 \rightarrow ^7F_6$ — from $I_{489}/I_{493} = 1.4$ to $I_{484}/I_{493} = 1.1$. Thus, the intensity of low-energy 547 nm satellite grows more than that of 493 nm satellite. Intensity of all FL bands grows thanks to an increase in concentration of Tb^{3+} and in crystallinity of the lattice (reduction of specific crystallite surface, reduction of strain) (Table) (for details, see [15]). It is known that for $Y_2O_3:Tb(5 \text{ mol}\%)$ system during drying at 100–300°C, FL bands have no doublets when crystallite sizes are up to 6 nm, and at 500°C, doublets occur when the crystallite size more than 20 nm [2]. In [9], occurrence of 548 nm FL satellite is allegedly attributed to surface states. At the same time, it should be noted that earlier in [10] an effect of considerable increase in the intensity of ~ 550 nm satellite with respect to ~ 542 nm baseband was observed when monoclinic $B-Gd_2O_3:Tb, Eu$ modification was formed after annealing at 1200°C. The monoclinic phase contained a trigonal Tb_7O_{12} impurity phase (space group $R\bar{3}$, ICSD 73822). Since the cubic $C-Gd_2O_3$ modification is

metastable up to $> 1200^\circ\text{C}$ [2,30,31], then it would appear reasonable that an increase in diffusion mobility of cations at this temperature according to Tamman effect may be followed by formation of clusters with structures, which are near-stable at high temperatures, of monoclinic $B\text{-Gd}_2\text{O}_3$ and trigonal Tb_7O_{12} phases. Concentration of Tb_7O_{12} is low for XRD phase analysis resolution, but is sufficient for FIR and RSS spectroscopy resolution. According to the set of optical studies, there are the following possible causes behind the relative increase in intensity of satellites and, to a greater extent, of the more intense $\sim 542\text{ nm}$ FL baseband after annealing at 1200°C .

1. Reduction of concentration of Tb^{4+} resulting in reduction of satellite quenching intensity of emission transitions ${}^5D_4 \rightarrow {}^7F_5$ and ${}^5D_4 \rightarrow {}^7F_6$ due to exchange interactions between Tb^{3+} and with Tb^{4+} . In this case, it is apparent that overlapping of intracenter FL concentration quenching on the general increase in the band intensity due to the higher degree of sample crystallinity will decrease considerably. This effect shall be present, because exchange interaction energy of $\text{Tb}^{3+} \leftrightarrow \text{Tb}^{4+}$ is considerably higher than that of $\text{Tb}^{3+} \leftrightarrow \text{Tb}^{3+}$. Therefore, intensity growth of FL baseband satellites will be ensured.

2. Presence of clusters with monoclinic $B\text{-Gd}_2\text{O}_3$ structure containing Tb^{3+} activator. In this case, the coordination number of cations grows up to 7, which facilitates more intense FL excitation. Change in the first coordination sphere of the cation activator in such clusters can certainly cause the occurrence and intensity growth of $\sim 550\text{ nm}$ satellite of 542 nm band.

3. Presence of clusters with Tb_7O_{12} structure containing a significant quantity of Tb^{3+} FL activator in centrosymmetric position C_{3i} , but with changed second environment sphere of Tb^{3+} , may also cause an increase in intensity of $\sim 550\text{ nm}$ satellite.

In this case, overlapping of the specified effects when the intensity of the studied FL band satellites is formed cannot be avoided.

Probably due to these changes, relative change in the intensity of FIR torsion and deformation bands in region B wave numbers $250\text{--}400\text{ cm}^{-1}$ is observed with transition to annealing at 1200°C . At the same time, in FIR spectrum, 498 cm^{-1} band that may be assigned to $(\text{Tb}^{4+}\text{-O}_x^{2-})$ groups disappears, but 141 cm^{-1} band occurs (translatory motion of Tb^{3+}). These facts correspond to the increase in concentration of Tb^{3+} and change in coordination sphere of O^{2-} environment. A substantial part of reduced Tb^{3+} is embedded in C_{3i} positions of Tb_7O_{12} clusters. This is indicated by the absence of changes in RSS spectrum which is not sensitive to centrosymmetric vibrational modes.

Similar effects were observed for annealing at 1200°C of $\text{Gd}_2\text{O}_3\text{:Tb, Eu}(2.5\text{ mol}\%)$ in air and hydrogen. Actually, $497\text{--}503\text{ cm}^{-1}$ band decreases and concentration of Tb^{4+} decrease considerably as result of reduction to Tb^{3+} . In another example, in hexagonal $\text{Gd}_2\text{O}_3\text{:Tb}(3, 5, 7\text{ mol}\%)$ which is rather similar in terms of the short-range order structure and has a similar stable group with center of

mass Gd_2O_3 , occurrence of 142 cm^{-1} band was detected in FIR spectrum after annealing at 1200°C , which was accompanied by transition of Tb^{4+} from crystallite surfaces with reduction to Tb^{3+} into crystallite volume into position C_{3i} [32].

Intensities of 315 and 347 cm^{-1} FIR bands typically increase almost by a factor of 3 while RSS band intensity in this region decreases compared with regions A and C. That means that the phonon state density in this region decreases and dipole bond moments increase. These effects coincide with sharp change in exchange interactions of Tb^{3+} and Tb^{4+} with decrease in concentration of the latter due to reduction and transition into the crystallite volume when crystallite sizes increase. It is not unlikely that the above effects are initiated by the change in these exchange interactions. Finally, only less effective exchange interactions of Tb^{3+} remain, which is reflected in FIR and RSS spectra (Figures 4 and 5) and in relative increase in FL intensity of doublet satellites of emission transitions ${}^5D_4 \rightarrow {}^7F_6$ (493 nm) and ${}^5D_4 \rightarrow {}^7F_5$ (549 nm).

5. Conclusion

When the annealing temperature of $(\text{Gd}_{0.97}\text{Tb}_{0.03})_x(\text{OH})_y(\text{CO}_3)_z \cdot n(\text{H}_2\text{O})$ sol-gel product increases from 800 to 1200°C , FL spectrum of the end product — $\text{Gd}_2\text{O}_3\text{:Tb}(3\text{ mol}\%)$ phosphor, changes. The main emission transitions of the intracenter FL of Tb^{3+} activator: ${}^5D_4 \rightarrow {}^7F_5$ and ${}^5D_4 \rightarrow {}^7F_6$, are represented by the corresponding ($489\text{:}493$) nm and ($543\text{:}547$) nm FL band doublets with annealing at 800°C and ($484\text{:}493$) nm and ($541\text{:}549$) nm FL band doublets with annealing at 1200°C . When the temperature increases, intensity of all doublets grows considerably due to higher degree of sample crystallinity and higher concentration of Tb^{3+} due to reduction of Tb^{4+} initiated by lack of equilibrium concentration of oxygen in air at high temperature. Intensities of low-energy satellites of these doublets increase considerably, more so for the FL transition band ${}^5D_4 \rightarrow {}^7F_5$.

These changes are caused by a decrease in quenching intensity of FL satellites of emission transitions ${}^5D_4 \rightarrow {}^7F_5$ and ${}^5D_4 \rightarrow {}^7F_6$ due to reduction of exchange interactions between Tb^{3+} and Tb^{4+} with considerable decrease in concentration of the latter. Moreover, similar effects may result from the presence of monoclinic $B\text{-Gd}_2\text{O}_3\text{:Tb}^{3+}$ impurity clusters and clusters with Tb_7O_{12} phase structure, which form low-energy FL band satellites owing to the change of their structure from bixbyite type cubic $C\text{-Gd}_2\text{O}_3$. According to the analysis of a set of changes in FL, FIR, RSS and DR spectra, the detected intensity ratio change effects of FL basebands and their low-energy satellites are described by the specific re-distribution of Tb^{4+} with reduction to Tb^{3+} from the crystal surfaces into their volume primarily into centrosymmetric position C_{3i} of cluster lattice cations of Tb_7O_{12} impurity. BG structure after annealing

at 800°C was found to contain degenerate Tb⁴⁺ *p*-type zone and degenerate Tb³⁺ *n*-type zone. BG width is equal to 2.55 eV with direct charge transitions. After sample annealing at 1200°C, BG is represented by two regions of direct charge transitions with excitation energy variation. With low excitation energies, direct transition is observed: degenerate *p*-type zone — degenerate *n*-type zone with $E_g = 2.56$ eV. With high excitation energies, *p*-type zone degeneration is removed due to charge re-compensation and direct transition is observed: valence band — degenerate *n*-type zone with $E_g = 3.4$ eV.

Acknowledgments

The authors would like to express their gratitude to B.A. Kolesov for Raman scattering spectra recording, to I.V. Korolkov for X-ray phase analysis, L.A. Sheludyakova for far IR-spectra recording.

Funding

The study was supported by the Ministry of Science and Higher Education of the Russian Federation, projects: No. 121031700315-2).

Conflict of interest

The authors declare that they have no conflict of interest.

References

- [1] Z. Xu, J. Yang, Z. Hou, C. Li, C. Zhang, S. Huang, J. Lin. *Mater. Res. Bull.* **44**, 1850 (2009).
- [2] M.A. Flores-Gonzalez, G. Ledoux, S. Roux, K. Lebbou, P. Perriat, O. Tillement. *J. Solid. State. Chem.* **178**, 989 (2005).
- [3] X. Gao, C. Li, S. Li, H. Zhang, Z. Li, Y. Hong, J. Sun. *J. Luminescence* **190**, 457 (2017).
- [4] R. Hemam, L.R. Singh, S.D. Singh, R.N. Sharan. *J. Luminescence* **197**, 399 (2018).
- [5] R.S. Loitongbam, W.R. Singh, G. Phaomei, N.S. Singh. *J. Luminescence* **140**, 95 (2013).
- [6] M. Ou, B. Muteleta, M. Martini, R. Bazzi, S. Roux, G. Ledoux, O. Tillement, P. Perria. *J. Coll. Interf. Sci.* **333**, 684 (2009).
- [7] X. Zhu, Z. Zhou. *J. Luminescence* **188**, 589 (2017).
- [8] W.-C. Chien, Y.-Y. Yu, C.-C. Yang. *Mater. Des.* **31**, 1737 (2010).
- [9] A. de J.M. Ramírez, A.G. Murillo, F. de J.C. Romo, M.G. Hernández, D.J. Viguera, G. Chaderyron, D. Boyer. *Mater. Res. Bull.* **45**, 40 (2010).
- [10] V.V. Bakovets, I.P. Dolgovesova, T.D. Pivovarova, M.I. Rakhmanova. *FTT* **62**, 12, 2147 (2020). (in Russian).
- [11] M. Nazarov, Do Y. Noh. *J. Rare Earths* **28**, Spec. Issue, 1 (2010).
- [12] D. Li, W. Qin, S. Liu, W. Pei, Z. Wang, P. Zhang, L. Wang, L. Huang. *J. Alloys Comp.* **653**, 304 (2015).
- [13] F. Vratny. *J. Chem. Phys.* **34**, 1377 (1961).
- [14] A.F. Andreeva, V.A. Ogorodnik. *Phys. Status. Solidi. B* **117**, K57 (1983).
- [15] V.V. Bakovets, A.V. Sotnikov, A.Sh. Agazhanov, S.V. Stankus, E.V. Korotaev, D.P. Pishchur, A.I. Shkatulov. *J. Am. Ceram. Soc.* **101**, 4773 (2018).
- [16] V.V. Bakovets, T.D. Pivovarova, I.P. Dolgovesova, I.V. Korolkov, O.V. Antonova, S.I. Kozhemyachenko. *ZhOKh* **88**, 5, 850 (2018). (in Russian).
- [17] D. Bloor, J.R. Dean. *J. Phys. C* **5**, 1237 (1972).
- [18] Y. Repelin, C. Proust, E. Husson, M. Beny. *J. Solid State Chem.* **138**, 163 (1995).
- [19] V.V. Bakovets, I.P. Dolgovesova, T.D. Pivovarova, L.A. Sheludyakova. *FTT* **63**, 12, 2162 (2021). (in Russian).
- [20] J. Ibanez, J.Á. Sans, V. Cuenca-Gotor, R. Oliva, Ó. Gomis, P. Rodríguez-Hernandez, A. Munoz, U. Rodríguez-Mendoza, M. Velazquez, P. Veber, C. Popescu, F.J. Manjon. *Inorg. Chem.* **59**, 9648 (2020).
- [21] H. Guo, X. Yang, T. Xiao, W. Zhang, L. Lou, J. Mugnier. *Appl. Surf. Sci.* **230**, 215 (2004).
- [22] M.W. Urban, B.C. Cornilsen. *J. Phys. Chem. Solids* **48**, 5, 475 (1987).
- [23] J. Tauc, R. Grigorovici, A. Vancu. *Phys. State Solids* **15**, 627 (1966).
- [24] K.V. Shalimova, *Fizika poluprovodnikov. Energoatomizdat, M.* (1985). 392 p. (in Russian).
- [25] P. Kubelka, F. Munk. *Z. Techn. Phys.* **12**, 593 (1931).
- [26] N.W. Gray, M.C. Prestgard, A. Tiwaria. *Appl. Phys. Lett.* **105**, 2229033 (2014).
- [27] W.B. White. *Appl. Spectr.* **21**, 3, 167 (1967).
- [28] A.F. Andreeva, I.Ya Gilman. *ZhPS* **28**, 5b, 895 (1978). (in Russian).
- [29] E.S. Trofimova, V.A. Pustovarov, A.F. Zatsepin. *FTT* **61**, 5, 872 (2019). (in Russian).
- [30] P.P. Fedorov, M.V. Nazarkin, R.M. Zaklyukin. *Kristallografiya* **47**, 316 (2002). (in Russian).
- [31] C.L. Luyer, A. Garcia Murillo, E. Bernstein, J. Mugnier. *J. Raman Spectr.* **34**, 234 (2003).
- [32] V.V. Bakovets, V.V. Sokolov, I.P. Dolgovesova, T.D. Pivovarova, I.Yu. Filatova, M.I. Rakhmanova, I.V. Yushina, I.P. Asanov, A.V. Sotnikov. *FTT* **64**, 11, 1834 (2022). (in Russian).

Translated by E.Ilyinskaya